# Terahertz emission from surface optical rectification in n-InAs

M. Reid and R. Fedosejevs

Department of Electrical and Computer Engineering, University of Alberta, Edmonton, Canada

## ABSTRACT

Terahertz emission from n-type (100), (110) and (111) InAs crystals have been measured as a function of the sample orientation. Emission was excited using 120fs Ti:Sapphire laser pulses at an incident angle of $45^o$ with fluences of approximately $1-2mJ/cm^2$. The data is shown to match the behavior expected for optical rectification at the surface, with small contributions from bulk optical rectification and photo-carrier diffusion. Thus, at fluences employed in the present study, it appears that the dominant mechanism for generating THz radiation is optical rectification at the surface.

**Keywords:** Optical Rectification, Terahertz, InAs, Surface Nonlinear Optics

## 1. INTRODUCTION

Techniques for generating radiation in the Terahertz (THz) frequency band are of increasing interest today, due to a growing number of applications, for example, in imaging,[1,2] biomedicine[3] and illicit drug-detection,[4] which exploit this radiation. In these application areas, one of three kinds of emitters are typically used for generating pulsed Terahertz radiation: (i) photoconductive emitters,[5,6] (ii) nonlinear optical generation by optical rectification[7] and (iii) semiconductor surface emission.[8]

Semiconductor surface emitters have been traditionally understood to generate radiation at low excitation fluences ($\lesssim 100nJ/cm^2$) by re-radiation due to dipole formation via transient currents. The transient currents are generated by an ultrafast excitation laser pulse either as a result of injected photo-carrier diffusion[9] normal to the sample surface or by the acceleration of photo-generated carriers in the surface depletion field.[8,10] However, when driven by very strong excitation fluences ($\gtrsim 100\mu J/cm^2$), it has been observed that there exists a strong contribution to the radiated THz field from the bulk nonlinear optical response of the emitter in wide-band gap materials such as InP,[11] as well as contributions from surface optical rectification.[12]

Of the semiconductor surface emitters reported in the literature, InAs has proven to generate relatively high levels of Terahertz radiation, especially under the influence of the magnetic field.[13,14] Virtually all of the studies regarding InAs have previously been conducted at low excitation fluences ($\lesssim 1\mu J/cm^2$), where transient currents are expected to produce the majority of the Terahertz radiation. More recently it has been shown that the dominant emission mechanism from (100) n-InAs is surface optical rectification.[15]

The ultimate limitation on the radiated pulse amplitude from InAs is governed by the Physics of the emission process at high driving fields. Therefore, it is of interest to investigate the behavior of the emission under high excitation fluences. In this report, we investigate the emission of Terahertz radiation from (100), (110) and (111) InAs surfaces and demonstrate that the emission is dominated by a different process than reported for low excitation conditions. Specifically, we find that when driving the emitter at high incident fluences, the emission becomes dominated by *surface* optical rectification.

Further author information: (Send correspondence to R. Fedosejevs)
R. Fedosejevs: E-mail: rfed@ece.ualberta.ca, Telephone: 1 780 492 5330

Photonics North 2004: Optical Components and Devices, edited by John C. Armitage, Simon Fafard, Roger A. Lessard, George A. Lampropoulos, Proceedings of SPIE Vol. 5577 (SPIE, Bellingham, WA, 2004) 0277-786X/04/$15 · doi: 10.1117/12.567332

## 2. BACKGROUND

### 2.1. Photo-carrier contribution to the radiated THz field

Terahertz emission from semiconductor surfaces has been studied extensively at low excitation fluences.[13,14,16–18] In this context, the dominant emission mechanisms are generally understood to be photo-carrier diffusion[9] or acceleration of photo-generated carriers in the surface depletion field.[8,10] The physics is different for these two processes, however, the general nature of the radiation that is emitted as a consequence of either process can be understood from the point of view of a transient current. That is, the optically injected carriers either diffuse or accelerate in the depletion field, leading to a transient current. The transient current then radiates the Terahertz wave according to Maxwell's equations:

$$E_{THz} \propto \frac{\partial J_{transient}(t)}{\partial t} \tag{1}$$

In general, the transient current flows normal to the sample surface.[18] Typically, the depletion field width is significantly less than 1 $\mu$m for n-InAs,[18] such that the transient current can be regarded as a time-dependent dipole ($\lambda_{1THz} = 300\mu m$)at the dielectric-air interface. One can therefore show that there can be no s-polarized wave radiated from this type of emission process.[19] Moreover, as the THz field depends only on the direction and magnitude of the transient dipole, the radiation pattern must be angularly independent under rotation of the substrate about the surface normal. That is, the magnitude of the transient dipole depends on the injected carrier density, which is independent of the crystal orientation, provided that the substrate is not birefringent. InAs is a zincblende material which is not naturally birefringent.

In addition to this, the process of photo-carrier diffusion, or photo-carrier acceleration in the depletion field, is not expected to be polarization dependent, aside from polarization-dependent Fresnel reflectivity from the substrate surface. Under excitation from linearly s- or p-polarized pump radiation, the emission is expected to depend only on the injected carrier density (i.e. $J = J(n_{injected})$ ) in equation 1.

These main points with respect to the Terahertz emission from photo-carriers can be summarized as follows:

- Dependence on crystallographic orientation: Angularly independent
- Dependence on pump polarization: Depends only on optical pump coupling
- Output polarization: p-polarized THz emission only

### 2.2. Bulk optical rectification

Bulk optical rectification can contribute to the Terahertz emission from semiconductor surfaces in a reflection geometry.[11,12] In this section we will briefly outline the expected behavior for bulk optical rectification from InAs.

InAs is a zincblende crystal, possessing $\bar{4}$3m symmetry. As such, the second-order nonlinear response is described by a susceptibility tensor with only 3 non-vanishing tensor elements, all of which are equal: $\chi^{(2)}_{xyz} = \chi^{(2)}_{yzx} = \chi^{(2)}_{zxy}$. In order to determine the far-infrared polarization at frequency $\Omega$ of the InAs lattice that results from an optical field at frequency $\omega$ we compute:

$$\mathbf{P}^{(2)}_{NL}(\Omega) = \chi^{(2)}(\Omega, -\omega, \omega) : \mathbf{E}_{opt}(-\omega)\mathbf{E}_{opt}(\omega) \tag{2}$$

As the polarization depends on the orientation of $\mathbf{E}_{opt}(\omega)$ with respect to the crystal axes, it is useful to transform the coordinate system to the beam coordinate system. Defining the $(\hat{s}, \hat{k}, \hat{z})$ coordinate system,[20] such that the $\hat{s}$ axis is in the surface of the crystal and parallel to an input s-polarized pump beam, $\hat{z}$ is normal to the crystal surface and $\hat{x} = \hat{z} \times \hat{s}$, we can define a rotation matrix from crystallographic coordinates to the beam coordinate system for each of the crystal faces, $R^{xtal}$: (111), (110) and (100) studied in the present report. For the bulk contribution to the radiated field, we are interested in the dependence of the THz field amplitude under

**Table 1.** THz field strengths for different polarization combinations expected for bulk optical rectification from zincblende crystals with $\bar{4}3m$ symmetry in reflection geometry. Combinations are listed as $E_{in,out}$.

**Radiated field strengths for different polarization combinations**

(111) **crystal face**

$$E^{THz}_{p,p} = \frac{1}{\sqrt{3}} A_p L_{eff} \Omega d_{14} t_p^2 E_p^2 \left[ \left(2F_s f_s^2 - F_s f_c^2 + 2F_c f_s f_c\right) - \left(\sqrt{2} F_c f_c^2\right) cos(3\phi) \right]$$
$$E^{THz}_{p,s} = \sqrt{\frac{2}{3}} A_s L_{eff} \Omega d_{14} t_p^2 f_c^2 E_p^2 sin(3\phi)$$
$$E^{THz}_{s,p} = \frac{1}{\sqrt{3}} A_p L_{eff} \Omega d_{14} E_s^2 t_s^2 \left[ F_s - \sqrt{2} F_c cos(3\phi) \right]$$
$$E^{THz}_{s,s} = -\sqrt{\frac{2}{3}} A_s L_{eff} \Omega d_{14} t_s^2 E_s^2 sin(3\phi)$$

(100) **crystal face**

$$E^{THz}_{p,p} = A_p L_{eff} \Omega d_{14} t_p^2 E_p^2 \left[ 2F_c f_s f_c - F_s f_c^2 \right] cos(2\phi)$$
$$E^{THz}_{p,s} = -4 A_s L_{eff} \Omega d_{14} t_p^2 E_p^2 f_s f_c sin(2\phi)$$
$$E^{THz}_{s,p} = A_p L_{eff} \Omega d_{14} F_s t_s^2 E_s^2 cos(2\phi)$$
$$E^{THz}_{s,s} = 0$$

(110) **crystal face**

$$E^{THz}_{p,p} = A_p L_{eff} \Omega d_{14} t_p^2 E_p^2 \left[ \left(2F_s f_s f_c - F_c f_s^2\right) sin(\phi) + \left(3F_c f_c^2\right) cos^2(\phi) sin(\phi) \right]$$
$$E^{THz}_{p,s} = A_s L_{eff} \Omega d_{14} t_p^2 E_p^2 \left[ \frac{1}{4} f_c^2 \left(cos(\phi) + 3cos(3\phi)\right) - f_s^2 cos(\phi) \right]$$
$$E^{THz}_{s,p} = A_p L_{eff} \Omega d_{14} t_s^2 E_s^2 F_c \left(sin(\phi) - 3sin(3\phi)\right)$$
$$E^{THz}_{s,s} = 3 A_s L_{eff} \Omega d_{14} t_s^2 E_s^2 cos(\phi) sin^2(\phi)$$

crystal rotation. We define another rotation matrix, $R^{rot}(\phi)$, that defines the angle of rotation of the crystal about it's surface normal. For the (111) crystal face, $\phi$ is defined as the angle between the $\hat{x}$ axis and the crystal $[\bar{2}11]$ axis. For the (110) face, $\phi$ is defined as the angle between the $\hat{x}$ axis and the crystal $[1\bar{1}0]$ axis. For the (100) crystal face, $\phi$ is defined as the angle between $\hat{x}$ and the crystal $[01\bar{1}]$ axis. From this, we can compute the susceptibility tensor in the beam coordinate system as a function of $\phi$ by applying the tensor transformation properties of a third rank tensor, and using the total transformation $R^{tot} = R^{rot} R^{xtal}$:

$$\chi^{(2)}_{ijk} = \sum_{lmn} \left( R^{tot}_{il} R^{tot}_{jn} R^{tot}_{km} \chi^{(2)}_{lmn} \right) \tag{3}$$

Using the susceptibility from Eq. 3 in Eq. 2, the independent lattice polarizations can be found. In turn, the s-polarized and p-polarized radiation resulting from the lattice polarization is readily obtained. The results are tabulated for the different polarization combinations, listed as $E_{in,out}$, in Table 1. The coefficients $f_s, f_c, t_s, t_p, A_s, A_p, F_s$, and $F_c$ given in Table 1 are as defined by Hübner et. al.[21] They depend on the angle of incidence and the linear optical properties of the material. $L_{eff}$ and $d_{14}$ represent the effective coherence length and the only non-vanishing second order tensor element respectively. The important points here are summarized as follows:

- Dependence on crystallographic orientation: Angularly independent and angularly dependent contributions to s- and p-polarized THz emission
- Dependence on polarization: Both s- and p- polarized THz emission depend on pump polarization
- Output polarization: Both s- and p-polarized fields will be radiated

**Table 2.** THz field strengths for different polarization combinations expected for surface optical rectification. Combinations are listed as $E_{in,out}$.

**Radiated field strengths for different polarization combinations**

(111) **crystal face**

$$
\begin{aligned}
E_{p,p}^{THz} &= A_p i\Omega E_p^2 \left[\epsilon(\Omega)\delta_{31}F_s f_c^2 - 2\delta_{15}f_s F_c f_c + \epsilon(\Omega)\delta_{33}F_s f_s^2 - \left(\delta_{11}F_c f_c^2\right) cos(3\phi)\right] \\
E_{p,s}^{THz} &= A_s i\Omega E_s^2 \delta_{11} f_c^2 sin(3\phi) \\
E_{s,p}^{THz} &= A_p i\Omega E_s^2 \left[F_s\delta_{31}\epsilon(\Omega) + (\delta_{11}F_c)\, cos(3\phi)\right] \\
E_{s,s}^{THz} &= -A_s i\Omega E_s^2 \delta_{11} sin(3\phi)
\end{aligned}
$$

(100) **crystal face**

$$
\begin{aligned}
E_{p,p}^{THz} &= A_p i\Omega E_p^2 \left[\epsilon(\Omega)\delta_{31}F_s f_c^2 - 2\delta_{15}f_s F_c f_c + \epsilon(\Omega)\delta_{33}F_s f_s^2\right] \\
E_{p,s}^{THz} &= 0 \\
E_{s,p}^{THz} &= A_p i\Omega E_s^2 F_s \delta_{31}\epsilon(\Omega) \\
E_{s,s}^{THz} &= 0
\end{aligned}
$$

(110) **crystal face**

$$
\begin{aligned}
E_{p,p}^{THz} &= A_p i\Omega E_p^2 \left[\left(\tfrac{1}{2}\epsilon(\Omega)\left(\delta_{31}-\delta_{32}\right)F_s f_c^2 - \left(\delta_{15}+\delta_{24}\right)f_s F_c f_c + \epsilon(\Omega)\delta_{33}F_s f_s^2\right)\right] \\
&\quad + A_p i\Omega E_p^2 \left[\left(\tfrac{1}{2}\epsilon(\Omega)\left(\delta_{31}-\delta_{32}\right)F_s f_c^2 - \left(\delta_{15}-\delta_{24}\right)f_s F_c f_c\right) cos(2\phi)\right] \\
E_{p,s}^{THz} &= A_s i\Omega E_p^2 \left(\delta_{15}-\delta_{24}\right) f_s f_c sin(2\phi) \\
E_{s,p}^{THz} &= A_p i\Omega E_s^2 \left[\tfrac{1}{2}\epsilon(\Omega)\left(\delta_{31}+\delta_{32}\right)F_s - \tfrac{1}{2}\epsilon(\Omega)\left(\delta_{31}-\delta_{32}\right)F_s cos(2\phi)\right] \\
E_{s,s}^{THz} &= 0
\end{aligned}
$$

## 2.3. Surface optical rectification

In the early 60's it was shown that nonlinear wave mixing can be generated at an interface.[22,23] Since this time, second-harmonic generation has been investigated as a surface-specific measurement technique.[24] As the bulk contribution typically dominates the second-harmonic signal in materials that lack inversion symmetry, this method has traditionally been used to investigate materials with inversion symmetry.[24]

Second-harmonic generation and optical rectification are essentially the same process, one occurring at the sum frequency, the other at the difference frequency of excitation. As such, the functional dependence of the emission on symmetry of the underlying medium is the same. Sipe and van Driel[20] have generated a phenomenological model for the surface contribution to second-harmonic generation. The expected results for the various InAs crystal faces and polarization combinations are listed in Table 2. The coefficients $f_s, f_c, t_s, t_p, A_s, A_p, F_s$, and $F_c$ given in Table 2 are as defined by Sipe and van Driel.[20] They depend on the angle of incidence and the linear optical properties of the material. The constants $\delta_{i,j}$ represent the phenomenological surface tensor elements, $\Omega$, in our case, is the far-infrared radiation frequency and $\epsilon(\Omega)$ is the far-infrared dielectric function, in our case, for InAs.

The results from Table 2 can be summarized as follows:

- Dependence on crystallographic orientation: Angularly independent and angularly dependent contributions to s- and p-polarized THz emission
- Dependence on polarization: Both s- and p- polarized THz emission depend on pump polarization
- Output polarization: Both s- and p-polarized fields will be radiated

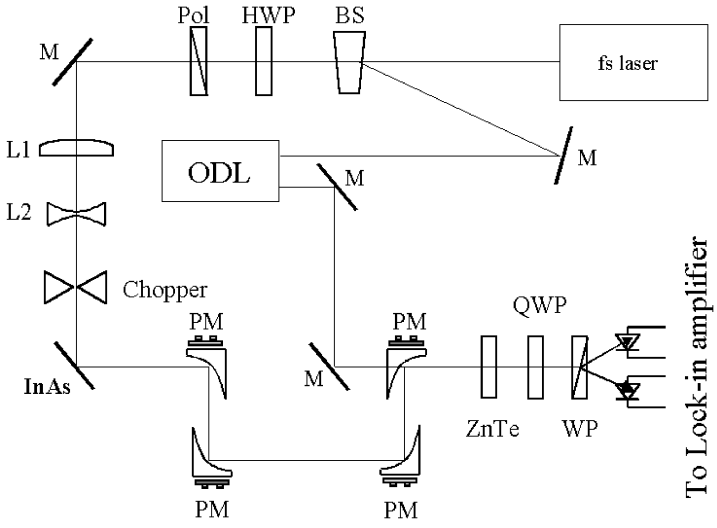


**Figure 1.** Schematic diagram of the THz system used in the experiments. FM is a flip mirror, pol is a polarizer, BS is a wedged beam splitter, PM are parabolic mirrors, QWP and HWP are quarter and half-wave plates respectively, WP is a Wollaston prism, L1 and L2 are +50 and -15cm focal length lenses. The InAs samples are either (100), (110) or (111) oriented, nominally undoped, n-InAs samples.

## 3. EXPERIMENTAL SET-UP

The experimental set-up is shown in Fig. 1. A regeneratively amplified Ti:Sapphire laser system (Spectra Physics Hurricane) is used as a source, operating at a center wavelength of 800 nm, at 1 kHz repetition rate, and a pulse-width of 130 fs (Gaussian FWHM). The beam is split into pump (92%) and probe (4%) beams using a wedged window. The probe is delayed with respect to the pump using an optical delay line, allowing time-resolved mapping of the THz field. A variable attenuator ($\lambda/2$ plate and polarizer) is used in the pump beam to vary the fluence. The THz radiation from the emitter is collected and imaged onto the detector using 4 F/2 parabolic mirrors in an f-2f-f geometry. The four parabolic mirrors are employed to attain an intermediate focal plane for testing samples, which is not used for the present study. To detect the THz radiation, the probe is co-linearly propagated through a 1mm thick, (110) ZnTe electro-optic crystal, with the THz field. This induces a polarization modulation, which is analyzed using a polarization bridge ($\lambda/4$ plate and Wollaston prism), with the differential photodiode signal detected using a lock-in amplifier at the optical chopping frequency of approximately 330Hz. The orientation of the $[00\bar{1}]$ axis of the ZnTe crystal is chosen to maximize the electro-optic signal for either the s- or p-polarized radiated THz field.[25] The (100) InAs emitter is nominally undoped, n-type InAs sample ($n_c = 1.9 \times 10^{16} cm^{-3}$, $\mu_H = 2.5 \times 10^4 cm^2 V^{-1} s^{-1}$) which is illuminated at 45 degrees angle of incidence. The (111) and (110) samples are also nominally undoped, n-type InAs ($n_c = 1.9 \times 10^{16} cm^{-3}$ and $\mu_H = 22000 cm^2 V^{-1} s^{-1}$ for the (110) crystal and $n_c = 3.2 \times 10^{16} cm^{-3}$ and $\mu_H = 18434 cm^2 V^{-1} s^{-1}$ for the (111) crystal). The pump beam is telescoped to a $1/e^2$ intensity beam diameter of $2.85 \pm 0.05$ mm for both emitters using a pair of lenses as shown in Fig. 1.

## 4. RESULTS

### 4.1. InAs (100)

In a previous report,[15] it was shown that the THz emission from (100) InAs at high excitation fluence is dominated by the contribution from the surface nonlinear response. This will be briefly reviewed here, such that the THz emission from the (110) and (111) face can be understood. The THz emission from n-InAs (100) was examined as a function of the azimuthal angle, $\phi$, defined as the angle the projection of the linearly p-polarized pump beam in the (100) plane makes with the $[01\bar{1}]$ crystal axis. The results are presented in Fig. 2.

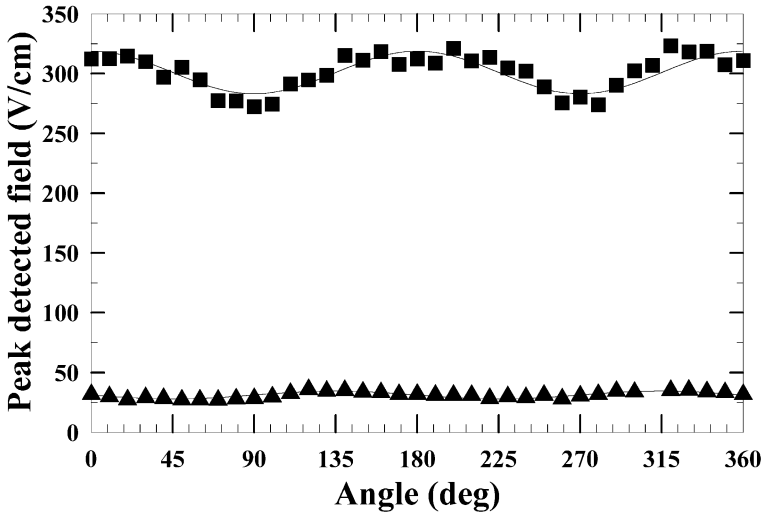


**Figure 2.** Peak detected THz field radiated from n-InAs (100) as a function of the azimuthal angle $\phi$, defined as the angle the projection of the linearly p-polarized pump beam in the (100) plane makes with the $[01\bar{1}]$ crystal axis. The data is taken at an incident fluence of approximately $2mJ/cm^2$. P- (squares) and s-polarized (triangles) peak THz fields are plotted.

For the (100) crystal face, excited at an angle of incidence of $45^o$, we observe a large angularly independent contribution to the p-polarized THz emission, with a small azimuthal dependence modulating this angularly independent contribution. In addition, there is virtually no s-polarized THz emission. The small contribution to the s-polarized THz emission amounts to approximately 1% in power relative to the p-polarized THz emission.

The two-fold rotational signal that modulates the large angularly independent contribution shown in Fig. 2 has the appropriate crystallographic dependence to suggest it is a result of bulk optical rectification. However, the peak-to-peak modulation is only about 20% of the angularly independent contribution, which suggests that the main emission mechanism is not bulk optical rectification.[15]

As the THz emission from photo-carrier related effects should not exhibit a strong dependence on the linear polarization of the pump beam (see section 2.1), the dependence of the THz emission from n-InAs(100) on pump-beam polarization was examined. In this case, the angle of the linear polarization was varied, while monitoring the radiated s- and p-polarized peak THz emission. The angle, $\theta$ is defined as the angle the linearly polarized pump beam makes with the p-polarized axis. That is, $\theta = 0$ corresponds to a linearly p-polarized pump beam, while $\theta = 90^o$ corresponds to a linearly s-polarized pump beam. The results are presented in Fig. 3. As discussed in section 2.1, it is not expected that photo-carrier effects will be substantially affected by polarization of the pump beam, aside from Fresnel effects. In fact, it can be shown that Fresnel coupling effects alone cannot account for the modulation observed in the p-polarized THz emission from (100) InAs presented in Fig. 3.[15] In addition, photo-carrier effects are not expected to produce s-polarized THz emission for the present geometry, under pump polarization rotation (see sec. 2.1). Therefore, the results in Fig. 3 suggest that photo-carrier effects do not dominate the emission.

The results tabulated in Table 2 are sufficient to explain the main features of the experimental results in Figures 3 and 2. For the (100) crystal face, the main observations that have to be explained for any mechanism responsible for the emission are: (i) An angularly independent p-polarized THz signal and no s-polarized THz signal under crystal rotation (c.f. Fig. 2), (ii) a large p- and s- polarized THz signal under linear pump polarization rotation (c.f. Fig. 3) and (iii) a $45^o$ phase shift in the signals for s- and p- polarized THz radiation under pump polarization angle rotation (c.f. Fig. 3).

First, the large angularly independent contribution to the radiated THz field under crystal rotation for the

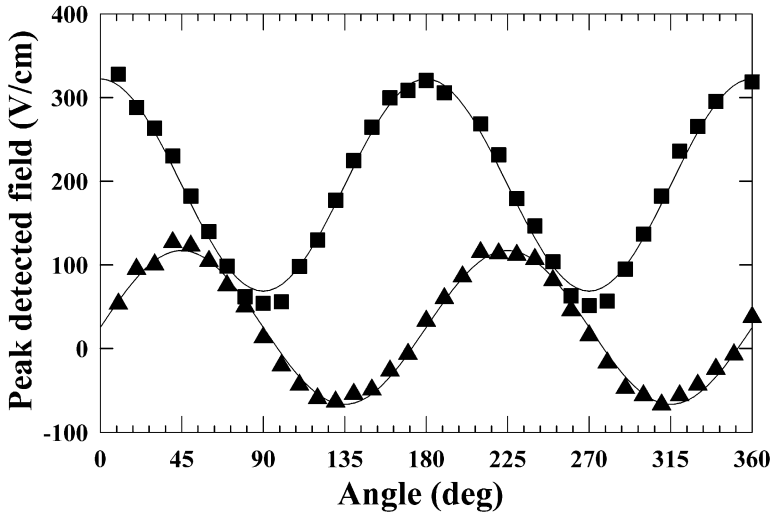


**Figure 3.** Peak detected THz fields as a function of the linear polarization angle $\theta$, defined as the angle between the linear polarized pump beam and a p-polarized pump beam. S- (triangles) and p-polarized (squares) THz emission is measured at an incident flux of approximately $1.7 mJ/cm^2$.

p-polarized THz field observed in Fig. 2 is simply explained as $E_p^{THz} \propto \left(E_p^{pump}\right)^2$, and the negligible s-polarized THz signal explained as $E_s^{THz} \propto E_p^{pump} E_s^{pump} = 0$ from Table 2, explaining the observation (i) above.

Secondly, the large pump-polarization dependent contributions to the radiated field are simply described as $E_p^{THz} \propto c_1 \left(E_s^{pump}\right)^2 + c_2 \left(E_p^{pump}\right)^2 = c_3 + c_4 cos(2\theta)$ and $E_s^{THz} \propto c_1 E_s^{pump} E_p^{pump} = c_2 sin(2\theta)$, where $\theta$ is the angle the linearly polarized pump beam makes with a p-polarized pump beam. This also explains exactly the observed $45^o$ relative phase shift in the data sets of Fig. 3. Therefore this also explains observations (ii) and (iii) above.

Therefore the conclusion is that surface nonlinear optical response of the (100) InAs is the dominant emission mechanism at high driving fields. The emission from (110) and (111) orientations are examined next to see if they show similar behaviour.

### 4.2. InAs (110)

The THz emission from n-InAs (110) was examined as a function of the azimuthal angle, $\phi$, defined as the angle the projection of the linearly p-polarized pump beam in the (110) plane makes with the $[\bar{1}10]$ crystal axis. The results are presented in Fig. 4.

The following important observations can be made with respect to Fig. 4. The expected behavior for bulk optical rectification is qualitatively violated. That is, from Table 1, there should be no angularly independent contribution to the p-polarized THz field, and the functional dependence on the angle $\phi$ is incorrect. Again, the angularly independent term might be interpreted as being due to photo-carrier effects, however, the crystallographic orientation dependence is not what should be expected for photo-induced carrier emission or bulk optical rectification.

Comparing the expectation from bulk (Table 1) and surface (Table 2) optical rectification, we see that there is a qualitative difference in the expected behavior. Specifically, there is a large angularly independent contribution in the p-polarized THz emission from the surface, which cannot result from the bulk nonlinear term (see Table 1). In addition to this, the bulk nonlinear term is expected to be of the form: $E_p^{THz} \propto c_1 sin(\phi) + c_2 cos^2(\phi) sin(\phi)$, where the angle $\phi$ is measured with respect to the $[\bar{1}10]$ crystal axis. Contrast this to the expected form for *surface* nonlinear optical response (see Table 2): $E_p^{THz} \propto c_1 + c_2 cos(2\phi)$, where the angle $\phi$ is also measured with respect to the crystal $[\bar{1}10]$ axis. Clearly, the $sin(\phi)$ dependence is incorrect qualitatively. The solid curve in Fig.

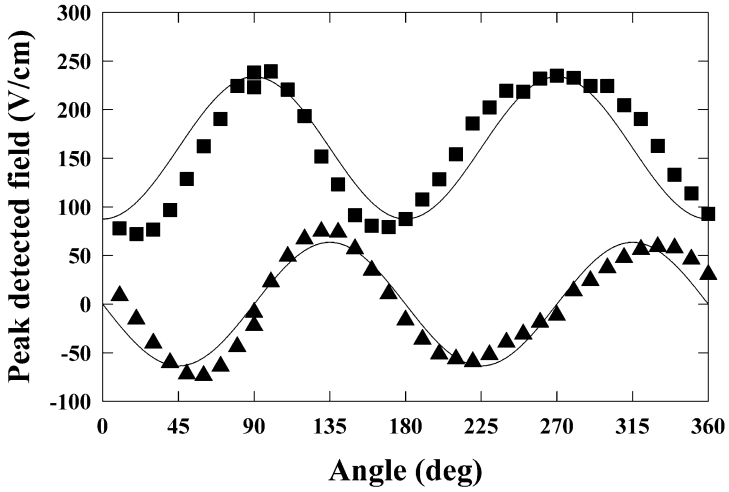


**Figure 4.** Peak detected THz field radiated from n-InAs (110) as a function of the azimuthal angle $\phi$, defined as the angle the projection of the linearly p-polarized pump beam in the (110) plane makes with the $[\bar{1}10]$ crystal axis. The data is taken at an incident fluence of approximately 1 $mJ/cm^2$. P- (squares) and s-polarized (triangles) peak THz fields are plotted.

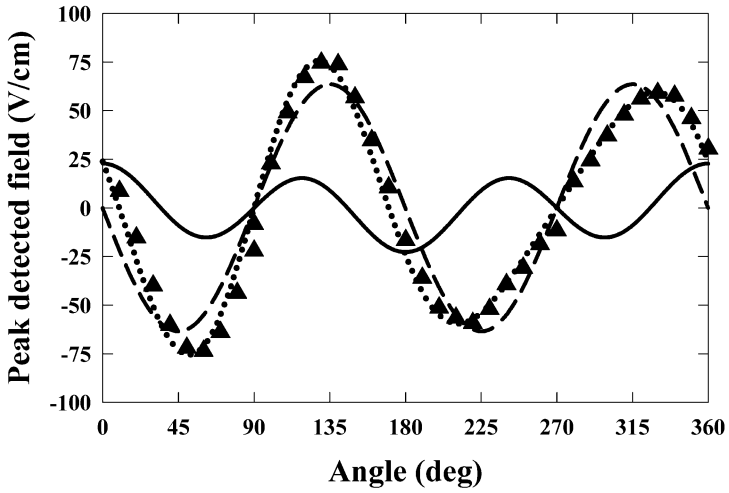


**Figure 5.** Peak detected s-polarized THz field radiated from n-InAs (110) as a function of the azimuthal angle $\phi$, defined as the angle the projection of the linearly p-polarized pump beam in the (110) plane makes with the $[\bar{1}10]$ crystal axis. The data is taken at an incident fluence of approximately 1 $mJ/cm^2$. See text for explanations of solid, dashed and dotted lines.

4 is a fit to the data using the expected behavior for surface optical rectification (i.e. $E^{THz}_{p,detected} = c_1 + c_2 cos(2\phi)$ ). Note that the curve fits the data reasonably well, but that there is an observable discrepancy. This discrepancy is explained by the fact that we expect a contribution to the radiated field due to bulk optical rectification on the order of 20%, as observed for the (100) crystal face (c.f. small modulation on angularly independent contribution in Fig. 2). The addition of the bulk term will skew the measured signals as the functional dependence is different for the two processes.

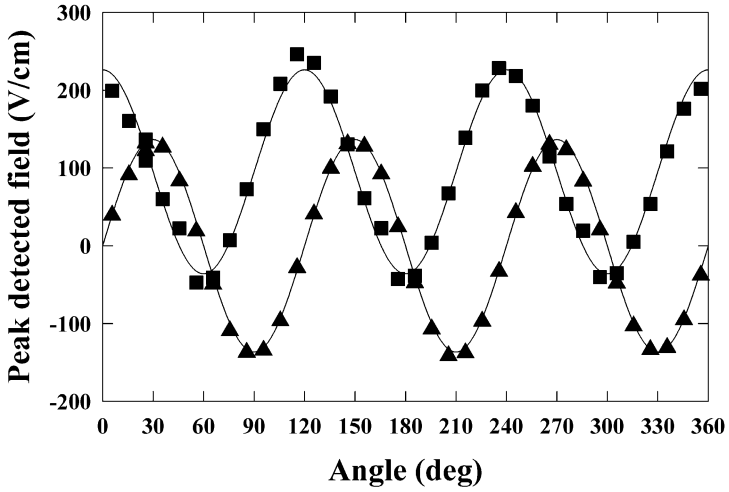


**Figure 6.** Peak detected THz field radiated from n-InAs (111) as a function of the azimuthal angle $\phi$, defined as the angle the projection of the linearly p-polarized pump beam in the (111) plane makes with the $[\bar{2}11]$ crystal axis. The data is taken at an incident fluence of approximately 1 $mJ/cm^2$. P- (squares) and s-polarized (triangles) peak THz fields are plotted. The solid curves are fits to the data based on the theoretical prediction for either surface or bulk optical rectification from Tables 2 or 1, respectively.

If the s-polarized THz emission is considered (see Fig. 4), again we find a qualitative difference between the expected bulk and surface contributions. Here, we expect the bulk contribution to be of the form (see Table 1): $E_s^{THz} \propto c_1 cos(\phi) + c_2 cos(3\phi)$, where the angle is again measured relative to the $[\bar{1}10]$ axis. Contrast this with the expected behavior from the surface nonlinear contribution, expected to have the form (see Table 2): $E_s^{THz} \propto c_1 sin(2\phi)$, where the angle $\phi$ is defined as before. Clearly, the measured behavior is not what is expected for bulk optical rectification. The solid curve fitting the s-polarized THz data of Fig. 4 is of the form: $E_{s,detected}^{THz} = c_1 sin(2\phi)$, which describes the data quite well. Again, the deviation from the fit can be described as the smaller contribution from the bulk process.

To demonstrate explicitly that the deviation of the data from the expected curves in Fig. 4 may result from a smaller contribution due to bulk optical rectification, consider Fig. 5 for the s-polarized THz data only. The solid curve is what might be expected from bulk optical rectification: $E_{s,detected}^{THz} = c_1 cos(\phi) + c_2 cos(3\phi)$, whereas the long dashed curve represents what might be expected for surface optical rectification: $E_{s,detected}^{THz} = c_1 sin(2\phi)$. If we take the sum of the solid curve and the dashed curve, we obtain the dotted curve in Fig. 5. From this, it is evident that a contribution from bulk optical rectification may lead to the distortion in the data from the expected behavior for surface optical rectification. Similar results are obtained for the p-polarized THz emission. The observation that there is a contribution to the radiated field from bulk optical rectification is consistent with the small contribution from bulk optical rectification in Fig. 2, for the (100) crystal face.

### 4.3. InAs (111)

Using the experimental set-up shown in Fig. 1, the Terahertz emission was examined as a function of the azimuthal angle, $\phi$, defined as the angle the projection of the linearly p-polarized pump beam, in the (111) plane, makes with the $[\bar{2}11]$ crystal axis. The measured results are presented in Fig. 6 for an excitation fluence of approximately 1 $mJ/cm^2$ .

From the angular dependence shown in Fig. 6, it is clear that there is a large contribution to the radiated THz field from optical rectification processes. The solid curves in Fig. 6 are fits to the data of the form: $E_{p,pk}^{THz} = c_1 + c_2 cos(\phi)$ and $E_{s,pk}^{THz} = c_1 sin(\phi)$ for the p- and s-polarized THz emission respectively, obtained from either Table 1 or Table 2, which have the same dependence on the angle $\phi$. For the (111) orientation, the

angular dependence for bulk optical rectification and for surface optical rectification is the same. Therefore, the Terahertz emission from n-InAs would be consistent with emission resulting from bulk optical rectification as reported elsewhere for n-InAs and InSb at high excitation fluence.[26,27] However, the experiments done here cannot distinguish between surface and bulk optical rectification for the (111) InAs face. Since the emission from the (100) and (110) InAs crystal faces is dominated by surface optical rectification, and that the peak radiated fields are comparable from all three crystal faces, it seems likely that the dominant emission from the (111) InAs crystal face is also a result of surface optical rectification.

## 5. CONCLUSION

Previously, it has been difficult to separate the bulk and surface contributions to second-harmonic generation[24,28] and therefore investigations have primarily focussed on centrosymmetric media.[24] In the present report, it has been demonstrated that the surface nonlinear optical response of the material can be monitored through the detection of the fields generated by optical rectification. Specifically, at high fluences, the THz emission is dominated by the surface nonlinear optical response in InAs, which is a non-centrosymmetric material. Therefore the use of Terahertz emission from InAs surfaces may be a useful surface-specific technique for studying InAs interfaces.

In this report, results of Terahertz emission from n-InAs (111), (110) and (100) crystal faces were examined. The influence of crystallographic orientation and pump-polarization dependence were presented. Based on these dependencies, it was clear that the Terahertz emission could not be attributed to photo-carrier effects or the bulk nonlinear optical response of the InAs for the (110) and (100) crystal faces. The emission patterns were shown to match that expected from *surface* optical rectification. Further, the expected behavior from the (111) surface is also consistent with surface optical rectification as the dominant emission mechanism.

## ACKNOWLEDGMENTS

Financial support for the research provided by MPB Technologies, Inc. and the Natural Sciences and Engineering Research Council of Canada is gratefully acknowledged. One of the authors, M. Reid, would like to acknowledge partial financial support from iCORE.

## REFERENCES

1. D. Mittleman, R. Jacobsen, and M. Nuss, "T-ray imaging," *IEEE J. Sel. Top. Quant.* **2**, pp. 679–692, 1996.
2. A. Fitzgerald, E. Berry, N. Zinovev, G. Walker, M. Smith, and J. Chamberlain, "An introduction to medical imaging with coherent terahertz frequency radiation," *Phys. Med. Biol.* **47**, pp. R67–R84, 2002.
3. X.-C. Zhang, "Terahertz wave imaging: horizons and hurdles," *Phys. Med. Biol.* **47**, pp. 3667–3677, 2002.
4. K. Kawase, Y. Ogawa, Y. Watanabe, and H. Inoue, "Non-destructive terahertz imaging of illicit drugs using spectral fingerprints," *Opt. Express* **11**, pp. 2549–2554, 2003.
5. J. T. Darrow, X.-C. Zhang, and D. H. Auston, "Saturation properties of large-aperture photoconducting antennas," *IEEE J. Quantum Electron.* **28**, pp. 1607–1616, 1992.
6. D. H. Auston, K. P. Cheung, and P. R. Smith, "Picosecond photoconducting hertzian dipoles," *Appl. Phys. Lett.* **45**, pp. 284–286, 1984.
7. B. B. Hu, X.-C. Zhang, D. H. Auston, and P. R. Smith, "Free-space radiation from electro-optic crystals," *Appl. Phys. Lett.* **56**, pp. 506–508, 1990.
8. X.-C. Zhang and D. H. Auston, "Optoelectronic measurement of semiconductor surfaces and interfaces with femtosecond optics," *J. Appl. Phys.* **71**, pp. 326–338, 1992.
9. T. Dekorsy, H. Auer, H. J. Baker, H. G. Roskos, and H. Kurz, "Thz electromagnetic emission by coherent infrared-active phonons," *Phys. Rev. B.* **53**, pp. 4005–4014, 1996.
10. X.-C. Zhang, J. Darrow, B. Hu, D. Auston, M. Schmidt, P. Tham, and E. Yang, "Optically induced electromagnetic radiation from semiconductor surfaces," *Appl. Phys. Lett.* **56**, pp. 2228–2230, 1990.
11. P. Saeta, B. Greene, and S. Chuang, "Short terahertz pulses from semiconductor surfaces: The importance of bulk difference-frequency mixing," *Appl. Phys. Lett.* **63**, pp. 3482–3484, 1993.

12. S. Chuang, S. Schmitt-Ring, B. Greene, P. Saeta, and A. Levi, "Optical rectification at semiconductor surfaces," *Phys. Rev. Lett.* **68**, pp. 102–105, 1992.
13. C. Weiss, R. Wallenstein, and R. Beigang, "Magnetic-field-enhanced generation of terahertz radiation in semiconductor surfaces," *Appl. Phys. Lett.* **77**, pp. 4160–4162, 2000.
14. R. McLaughlin, A. Corchia, M. B. Johnston, Q. Chen, C. M. Ciesla, D. D. Arnone, G. A. C. Jones, E. H. linfield, A. G. Davies, and M. Pepper, "Enhanced coherent terahertz emission from indium arsenide in the presence of a magnetic field," *Appl. Phys. Lett.* **76**, pp. 2038–2040, 2000.
15. M. Reid and R. Fedosejevs, "Terahertz emission from (100) InAs surfaces at high excitation fluence," *Appl. Phys. Lett.* , Submitted, 2004.
16. N. Sarakura, H. Ohtake, S. Izumida, and Z. Liu, "High average-power thz radiation from femtosecond laser-irradiated InAs in a magnetic field and its elliptical polarization characteristics," *J. Appl. Phys.* **84**, pp. 654–656, 1998.
17. J. N. Heyman, P. Neocleous, D. Hebert, P. A. Crowell, T. Mueller, and K. Unterrainer, "Terahertz emission from gaas and inas in a magnetic field," *Phys. Rev. B.* **64**, pp. 0852021–0852027, 2001.
18. M. B. Johnston, D. M. Whittaker, A. Corchia, A. G. Davies, and E. H. Linfield, "Simulation of terahertz generation at semiconductor surfaces," *Phys. Rev. B.* **65**, pp. 1653011–1653018, 2002.
19. W. Lukosz, "Light emission by magnetic and electric dipoles close to a plane dielectric interface. iii. radiation patterns of dipoles with arbitrary orientation," *J. Opt. Soc. Am.* **69**, pp. 1495–1503, 1979.
20. J. Sipe, D. Moss, and H. van Driel, "Phenomenological theory of optical second- and third-harmonic generation from cubic centrosymmetric crystals," *Phys. Rev. B.* **35**, pp. 1129–1140, 1987.
21. W. Hübner, K. Bennemann, and K. Böhmer, "Theory for the nonlinear optical response of transition metals: Polarization dependence as a fingerprint of the electronic structure at suraces and interfaces," *Phys. Rev. B* **50**, pp. 17597–17605, 1994.
22. N. Bloembergen and P. Pershan, "Light waves at the baoundary of nonlinear media," *Phys. Rev.* **128**, pp. 606–622, 1962.
23. N. Bloembergen, R. Chang, S. Jha, and C. Lee, "Optical second-harmonic generation in reflection from media with inversion symmetry," *Phys. Rev.* **174**, pp. 813–822, 1968.
24. G. Lüpke, "Characterization of semiconductor interfaces by second-harmonic generation," *Surf. Sci. Rep.* **35**, pp. 75–161, 1999.
25. P. C. M. Planken, H.-K. Nienhuys, H. J. Bakker, and T. Wenckebach, "Measurement and calculation of the orientation dependence of terahertz pulse detection in ZnTe," *J. Opt. Soc. Am. B.* **18**, pp. 313–317, 2001.
26. P. Gu, M. Tani, S. Kono, K. Sakai, and X.-C. Zhang, "Study of terahertz radiation from InAs and insb," *J. Appl. Phys.* **91**, pp. 5533–5537, 2002.
27. S. Howells and L. Schlie, "Temperature dependence of terahertz pulses produced by difference-frequency mixing in InSb," *Appl. Phys. Lett.* **67**, pp. 3688–3690, 1995.
28. P. Guyot-Sionnest, W. Chen, and Y. Shen, "General considerations on optical second-harmonic generation from surfaces and interfaces," *Phys. Rev. B* **33**, pp. 8254–8263, 1986.